JUSTC

Article

http://justc.ustc.edu.cn

Received: December 28, 2024; Accepted: February 06, 2025

Hierarchically designed nacre-like composites with enhanced impact resistance

Qingsheng Zeng[1,2*], Jiahao Su[1,2*], Junlan Zhan[1], Pengfei Wang[1], Duohong Zou[2,3] ✉, and Huailing Gao[1] ✉

[1]*Hefei National Research Center for Physical Sciences at the Microscale, CAS Key Laboratory of Mechanical Behavior and Design of Materials, Department of Modern Mechanics, University of Science and Technology of China, Hefei 230026, China;*
[2]*Stomatological College of Anhui Medical University, The Affiliated Stomatological Hospital of Anhui Medical University, Key Lab of Oral Diseases Research of Anhui Province, Hefei 230032, China;*
[3]*Department of Oral Surgery, Shanghai Ninth People's Hospital, Shanghai Jiao Tong University School of Medicine; College of Stomatology, Shanghai Jiao Tong University; National Center for Stomatology; National Clinical Research Center for Oral Diseases; Shanghai Key Laboratory of Stomatology, Shanghai 200011, China*

* These authors contributed equally to this work
✉Correspondence: Duohong Zou, E-mail: zouduohongyy@163.com; Huailing Gao, E-mail: ghuailing@ustc.edu.cn

Graphical abstract

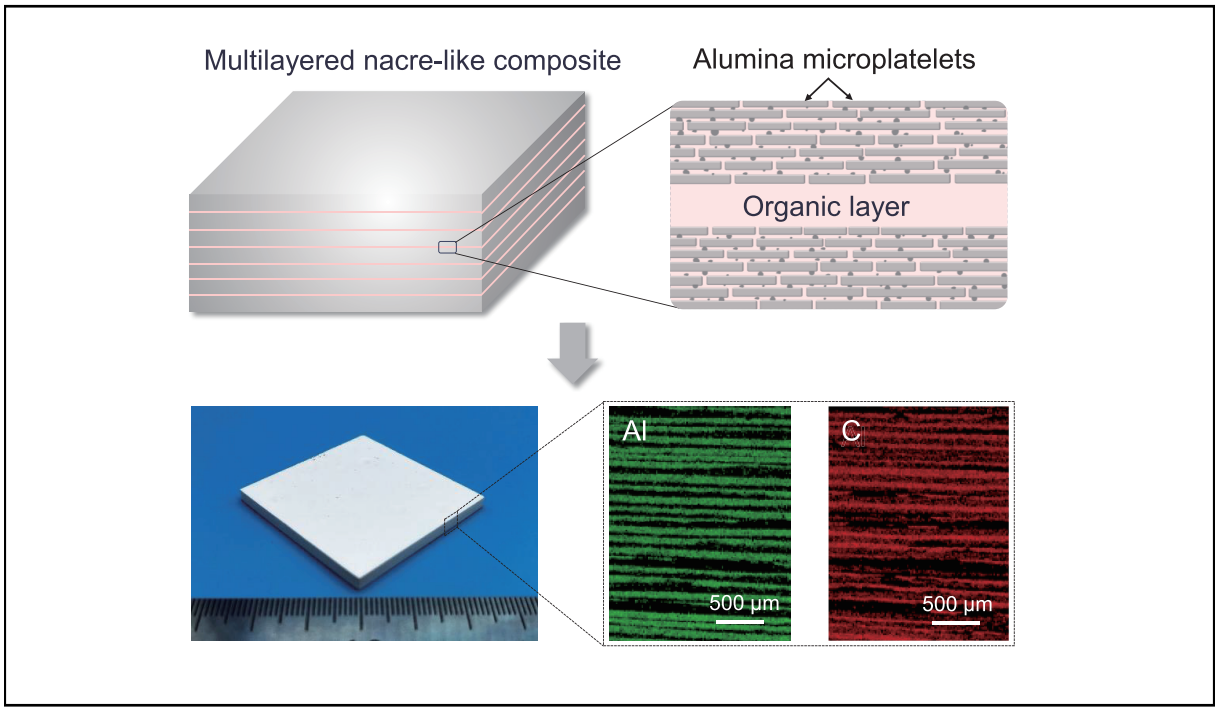

Nacre-like composites with enhanced dynamic impact resistance can be produced through a hierarchically laminated structural design.

Public summary

- Drawing inspiration from the hierarchical structure of biological composites, we produce multilayered nacre-like composites via a scalable bottom-up assembly strategy.
- The multilayered nacre-like composites feature a multilevel structure with a brick-and-mortar structure at the nanoscale and a multilayered rigid–soft laminate structure at the microscale.
- The multilayered nacre-like composites demonstrate both hierarchical toughening behavior under quasistatic loading conditions and greatly improved impact resistance under dynamic loading conditions.

Citation: Zeng Q S, Su J H, Zhan J L, et al. Hierarchically designed nacre-like composites with enhanced impact resistance. *JUSTC*, **2025**, 55(6): 0604. CSTR: 32290.14.JUSTC-2024-0163. DOI: 10.52396/JUSTC-2024-0163

JUSTC

Article

http://justc.ustc.edu.cn

Received: December 28, 2024; Accepted: February 06, 2025

Hierarchically designed nacre-like composites with enhanced impact resistance

Qingsheng Zeng[1,2*], Jiahao Su[1,2*], Junlan Zhan[1], Pengfei Wang[1], Duohong Zou[2,3] ✉, and Huailing Gao[1] ✉

[1]*Hefei National Research Center for Physical Sciences at the Microscale, CAS Key Laboratory of Mechanical Behavior and Design of Materials, Department of Modern Mechanics, University of Science and Technology of China, Hefei 230026, China;*
[2]*Stomatological College of Anhui Medical University, The Affiliated Stomatological Hospital of Anhui Medical University, Key Lab of Oral Diseases Research of Anhui Province, Hefei 230032, China;*
[3]*Department of Oral Surgery, Shanghai Ninth People's Hospital, Shanghai Jiao Tong University School of Medicine; College of Stomatology, Shanghai Jiao Tong University; National Center for Stomatology; National Clinical Research Center for Oral Diseases; Shanghai Key Laboratory of Stomatology, Shanghai 200011, China*

* These authors contributed equally to this work
✉Correspondence: Duohong Zou, E-mail: zouduohongyy@163.com; Huailing Gao, E-mail: ghuailing@ustc.edu.cn

Cite This: *JUSTC*, **2025**, 55(6): 0604 (8pp) Read Online SI Supporting Information

Abstract: Lightweight and mechanically robust composites are widely utilized as structural components in many different sectors. These structural components often face the challenge of dynamic impact loads. Therefore, research on how to improve the impact resistance of structural materials has always been highly important. In this study, on the basis of a scalable bottom-up assembly route, we prepare multilayered nacre-like composites with enhanced impact resistance. The multilayered nacre-like composites have a brick-and-mortar structure at the nanoscale and a rigid–soft laminate structure at the microscale. The experimental results revealed that the hierarchically designed composites demonstrated hierarchical toughening behavior under quasistatic loading conditions and exhibited greatly improved impact resistance under dynamic loading conditions. This study provides a theoretical basis for the relationship between the structure and dynamic mechanical properties of multilayered nacre-like composites and provides new ideas for the future research and development of impact-resistant composites.

Keywords: nacre-like composite; brick-and-mortar structure; laminate structure; impact resistance

CLC number: TB333 **Document code:** A

1 Introduction

Lightweight and mechanically robust composites have been extensively adopted as structural materials in a multitude of industries, with aircraft, automobiles, and protective armor being just a few prominent examples[1–6]. These applications highlight the importance of developing lightweight materials that can effectively combine high strength, high stiffness, and high toughness. High strength and stiffness allow structures to withstand mechanical loads without breaking down, whereas a high level of toughness is essential to guarantee slow and noncatastrophic disintegration of the structures when subjected to pressures exceeding their strength limits. In most application scenarios, sufficient impact resistance is highly important to withstand various dynamic impact loads that frequently stem from the external environment[7–10]. However, integrating these properties poses a significant challenge for most synthetic materials because they counteract one another[11,12].

Through millions of years of evolution in nature, the structures of biological materials have been meticulously refined. As a result, they integrate multiple mutually exclusive mechanical properties to meet the survival needs of organisms[13–16]. Consequently, researchers have extensively investigated the strengthening and toughening principles underlying these biological structures and incorporated them into artificial structural materials[17–19]. Among them, the nacreous layer of certain mollusks, composed of aragonite flakes and organic chitin interlayers, acts as a typical biological armor that is strong, tough and impact resistant, defending mollusks from predators. It has been widely studied and imitated, resulting in a series of high-performance nacre-like composites[20–28].

Notably, studies have revealed that introducing multilayered laminate structures into nacre-like composites can further effectively enhance their mechanical properties[29,30]. The brick-and-mortar structure connected with mineral bridges at the nanoscale enables composites with intrinsic toughness, whereas the rigid–soft laminate architecture at the microscale gives rise to a significant extrinsic toughening mechanism. Unfortunately, these studies focused only on the quasistatic mechanical performance of the resulting materials, and it remains uncertain how this multilevel structure affects the dynamic mechanical properties of these materials, such as their impact resistance[29].

In this work, we fabricated multilayered nacre-like composites via the scalable bottom-up assembly method we

CSTR: 32290.14.JUSTC-2024-0163
DOI: 10.52396/JUSTC-2024-0163
JUSTC, **2025**, 55(6): 0604

previously proposed[31]. The nacre-like composites feature a comparable multilevel structure as previously reported[29], which is considered to have the ability to achieve a combination of intrinsic toughening and extrinsic toughening. At the nanoscale, they possess a brick-and-mortar structure that is interconnected by mineral bridges. At the microscale, they exhibit a multilayered rigid–soft laminate structure, which is formed by integrating relatively rigid brick-and-mortar lamellae with relatively ductile polymer lamellae. Our experimental findings reveal that multilayered nacre-like composites can not only demonstrate hierarchical toughening in terms of quasistatic mechanical properties but also excellent dynamic mechanical properties. This work offers valuable insights for the development of impact-resistant composites.

2 Materials and methods

2.1 Reagents and materials

All the raw materials and reagents used in this study were sourced commercially and utilized without additional purification. The alumina microplatelets were sourced from Merck Biotech, the kaolin clay was obtained from Jiangxi Jianhong Ceramic Art Materials Wholesale Co., Ltd., the epoxy resin (EP) components A and B were purchased from Hubei Yongbang Taihe New Materials Co., Ltd., and the bacterial cellulose (BC) nanofiber dispersion (0.8 wt%) was acquired from Guilin Qihong Technology Co., Ltd.

2.2 Synthesis

2.2.1 Preparation of nacre-like composite films

The composite slurry was formulated by mixing alumina microplatelets, kaolin clay, and BC (0.8 wt%) dispersions with certain weight ratios. Initially, kaolin clay (1 g) was incorporated into distilled water (300 mL). The mixture was subsequently placed in a planetary activator via ball milling at 200 r/min for 8 h. Subsequently, alumina platelets (9 g) were incorporated into the mixture, and ball milling was carried out for an additional 4 h. After the ball milling process was completed, the slurry was moved to a beaker, and the BC dispersion (100 mL) was incorporated. The mixture was stirred mechanically at 400 r/min for 4 h. Following this, the thoroughly mixed slurry was transferred into Petri dishes with dimensions of 24 cm × 24 cm, with approximately 250 g of slurry allocated to each dish. The Petri dishes were placed on a hot plate set to 40 °C to facilitate the evaporation process. Following approximately 24 h of evaporation, the composite films were completely dried and meticulously removed from the Petri dishes. The films had a thickness of approximately 100 μm and were cut into smaller dimensions of approximately 5 cm × 5 cm and then stored for future use.

2.2.2 Preparation of ceramic frames (CFs)

First, the above composite films were divided into 1L, 2L, 4L, 8L, 16L, and 50L groups. For the 1L group, 50 layers of film were laminated together (1 part); for the 2L group, 24 layers of film were laminated together (2 parts); for the 4L group, 12 layers of film were laminated together (4 parts); for the 8L group, 6 layers of film were laminated together (8 parts); for the 16L group, 3 layers of film were laminated together (16 parts); and for the 50L group, only 1 layer of film was compacted (50 parts). Each pressing step was maintained at 40 MPa for 4 h at room temperature to promote the compaction of these stacked films and improve their flatness. The single-layer film and these laminated films were then transferred to a muffle furnace and sintered at 1600 °C for 3 h at a heating rate of 5 °C/min. Upon natural cooling, the resulting thickness of the single-layer CF was approximately 60 μm. These CFs originating from different layers of thin films were ready for subsequent use.

2.2.3 Preparation of multilayered nacre-like composites

The CFs (consisting of 50, 24, 12, 6, 3, and 1 layers) were stacked in quantities of 1, 2, 4, 8, 16, and 50 layers, correspondingly, to achieve a cumulative thickness of approximately 3 mm for each group. The EP was formulated by combining adhesives A and B at a 3∶1 mass ratio and ensuring thorough mixing. The stacked CFs were subsequently immersed in EP and maintained in a vacuum atmosphere for 30 min to promote resin infiltration into the internal pores of the CFs and the gaps between adjacent layers. The stacked CFs were subsequently removed from the EP solution, and a 564 g weight was placed above each CF for 24 h to ensure the curing of the EP. Next, the composites were subjected to grinding and polishing, ultrasonic rinsing, and drying, resulting in multilayered composites measuring approximately 40 mm × 40 mm × 3 mm.

2.2.4 Characterization and testing

Microscopic (OM) images were obtained via the dark-field mode of the YM710TR metallographic microscope. Scanning electron microscopy (SEM) images were obtained with a Guoyi Quantum SEM 3200 tungsten filament scanning electron microscope at an acceleration of 7 kV. Energy dispersive X-ray spectroscopy (EDS) images were obtained with a Carl Zeiss Supra 40 field-emission scanning electron microscope at an acceleration of 10 kV, which was equipped with an Ultim Max 100 probe. X-ray diffraction (XRD) patterns were acquired using a Philips X'Pert Pro Super X-ray diffractometer with Cu Kα radiation and a scanning speed of 0.2°/min. Small-angle X-ray scattering (SAXS) data were acquired via SAXSPoint 2.0 with a wavelength of 0.154 nm from 0.5° to 5°. Micro X-ray tomography (micro-CT) imaging was performed to characterize the internal damage morphologies of the nacre-like composites via an Always Imaging AX-2000 3D X-ray microscope operating at an accelerating voltage of 100 kV. Thermal gravity analysis (TGA) data were collected with a STA449F3 thermal analyzer from 30 to 800 °C with a heating rate of 10 °C/min and an air purge at a flow rate of 20 mL/min. The volume ratio of epoxy resin (%) was calculated with the aid of TGA via the following equation[31]:

$$\text{Volume ratio of epoxy resin} = \frac{[\,(m_1 - m_2)\,/\rho_1\,]}{[\,(m_1 - m_2)\,/\rho_1\,] + (m_2/\rho_2)},$$

where m_1 is the weight of the EP-infiltrated composite, m_2 is the weight after the EP-infiltrated composite burns at 800 °C, ρ_1 is the density of the EP, and ρ_2 is the density of the ceramic

CSTR: 32290.14.JUSTC-2024-0163
DOI: 10.52396/JUSTC-2024-0163
JUSTC, **2025**, 55(6): 0604

frame. The weight of the nacre-like composites was measured on an HZK-FA210S electronic balance, and the density (g/cm^3) of the nacre-like composites with different numbers of layers was calculated via the following formula:

$$\rho = \frac{m_3 \rho_{H_2O}}{m_1 - m_2},$$

where m_1 is the mass of the nacre-like composite in air after full water saturation, m_2 is the mass of the nacre-like composite fully saturated with water, m_3 is the mass of the dried nacre-like composite in air, and ρ_{H_2O} is the density of distilled water, which is 1 g/cm^3.

The compression test data were obtained via a DANA-10KN universal testing machine with a 10 kN load cell. All the samples were cut into cubes measuring ~ 3 mm × 3 mm × 3 mm, with the force applied perpendicular to the layer stacking direction. The tests of 50L composites were categorized into vertical and parallel orientations. (⊥) indicates the applied force perpendicular to the layers; (//) indicates the applied force parallel to the layers. The displacement rate was maintained at 1 mm/min. The data of three-point bending tests were obtained via a DANA-10KN universal testing machine with a 10 kN load cell. All the samples were cut into beam shapes with dimensions of ~ 20 mm × 2 mm × 3 mm, with the force applied perpendicular to the layer stacking direction. The support span was set to 12 mm, and the displacement rate was maintained at 1 mm/min. For the single-edge notched bending (SENB) tests, all the samples were cut into beam shapes with dimensions of ~ 20 mm × 3 mm × 3 mm. The notches were created via a 350 μm low-speed diamond wire cutting machine (STX-202a), followed by repeated sliding of a razor blade along the incision for sharpening. The displacement rate for the flexural tests was maintained at 1 mm/min, and the support span was 12 mm. The test video was obtained via a microscopic camera.

For the drop-ball rebound test, all the samples were cut into cuboids with dimensions of ~ 20 mm × 20 mm × 3 mm. Each sample was placed on a ground and kept horizontal. A steel ball weighing 2.1 g was released from a height of 50 cm above the sample. The rebound height of the steel ball was recorded via a camera with a vertically placed ruler as a reference. The energy dissipation ratio (%) was calculated on the basis of this rebound height via the following formula:

$$\text{Energy dissipation ratio} = \frac{h - h_1}{h} \times 100\%,$$

where h is the release height of the steel ball and h_1 is the rebound height of the steel ball after the first contact with the sample.

For the drop-hammer impact test, all the samples were cut into cuboids with dimensions of ~ 20 mm × 20 mm × 3 mm. Each sample was placed on a ground and kept horizontal. A 370 g semicircular hammer head with a diameter of 20 mm was dropped vertically onto the sample surface from a certain height, which was then inspected for fractures. If intact, the height was increased in increments of 5 mm, and this process continued until fracture occurred. The fracture height was recorded, and the fracture energy (J) was calculated via the following formula:

$$\text{Fracture energy} = mgh,$$

where m is the weight of the hammer, g is 9.8 m/s^2, and h is the height of the hammer's center of mass when it breaks the sample.

The dynamic mechanical analysis data were obtained via a TA Instruments RSA-G2 solid analyzer. All the samples were cut into beam shapes with dimensions of ~ 20 mm × 3 mm × 3 mm. The oscillation direction was oriented perpendicular to the layer stacking direction, with a test span of 10 mm, a test strain of 0.1%, and a test frequency range from 20 to 80 Hz at room temperature. The split Hopkinson pressure bar (SHPB) test data were acquired by a conventional SHPB device. All the samples were cut into cubes measuring ~ 6 mm × 6 mm × 6 mm, with the force applied perpendicular to the layer stacking direction. A pulse shaper was applied to modify the incident wave and remove the wave dispersion. The striker, incident bar, and transmit bar were made of ultraduralumin with a diameter of 14.5 mm, and the lengths were 200, 1000, and 800 mm, respectively.

3 Results and discussion

3.1 Microstructure of the multilayered nacre-like composites

In our research, the multilayered nacre-like composite was designed with a hierarchical structure (Fig. 1a), wherein the EP matrix infiltrated into the gaps between adjacent alumina microplatelets to form a brick-and-mortar structure at the nanoscale and between adjacent CF layers to form a multilayered rigid–soft laminate structure at the microscale. Alumina microplatelets with a diameter from a few to a dozen micrometers (Fig. S1 in Supporting information) were used as the main building blocks to resemble the nacre-like layered structure of natural nacre. We fabricated hierarchically structured nacre-like composites via a multilevel bottom-up assembly process (Fig. 1b, Fig. S2). The alumina microplatelets were first assembled with BC nanofibers and kaolin clay nanoparticles into nacre-like composite films, in which they were arranged in a layered stacking structure (Fig. S3). High-resolution SEM images (Fig. S3b and d) revealed that BC nanofiber networks connected the stacked alumina microplatelets. The BC content in the composite film was estimated to be approximately 9 wt% by TGA analysis (Fig. S4a). The composite films were then transformed into thin CF lamellae through sintering. The crystal phases of the alumina microplatelets and kaolin clay changed following sintering and transformed into the mullite phase (Fig. S4b), demonstrating their effective bonding. As shown in Fig. 1c, the arranged alumina microplatelets were welded together into a porous ceramic frame. After being stacked and infiltrated with the EP matrix, EP was alternately distributed among the pores of the CF, forming a brick-and-mortar structure at the nanoscale (Fig. 1d). At the microscale, we can find an organic layer bonding two neighboring brick-and-mortar lamellae with a robust interface formed between the EP matrix and the CF (Fig. 1e, Fig. S5). The density of the CFs increased after infiltration of EP and gradually decreased with increasing

CSTR: 32290.14.JUSTC-2024-0163
DOI: 10.52396/JUSTC-2024-0163
JUSTC, **2025**, 55(6): 0604

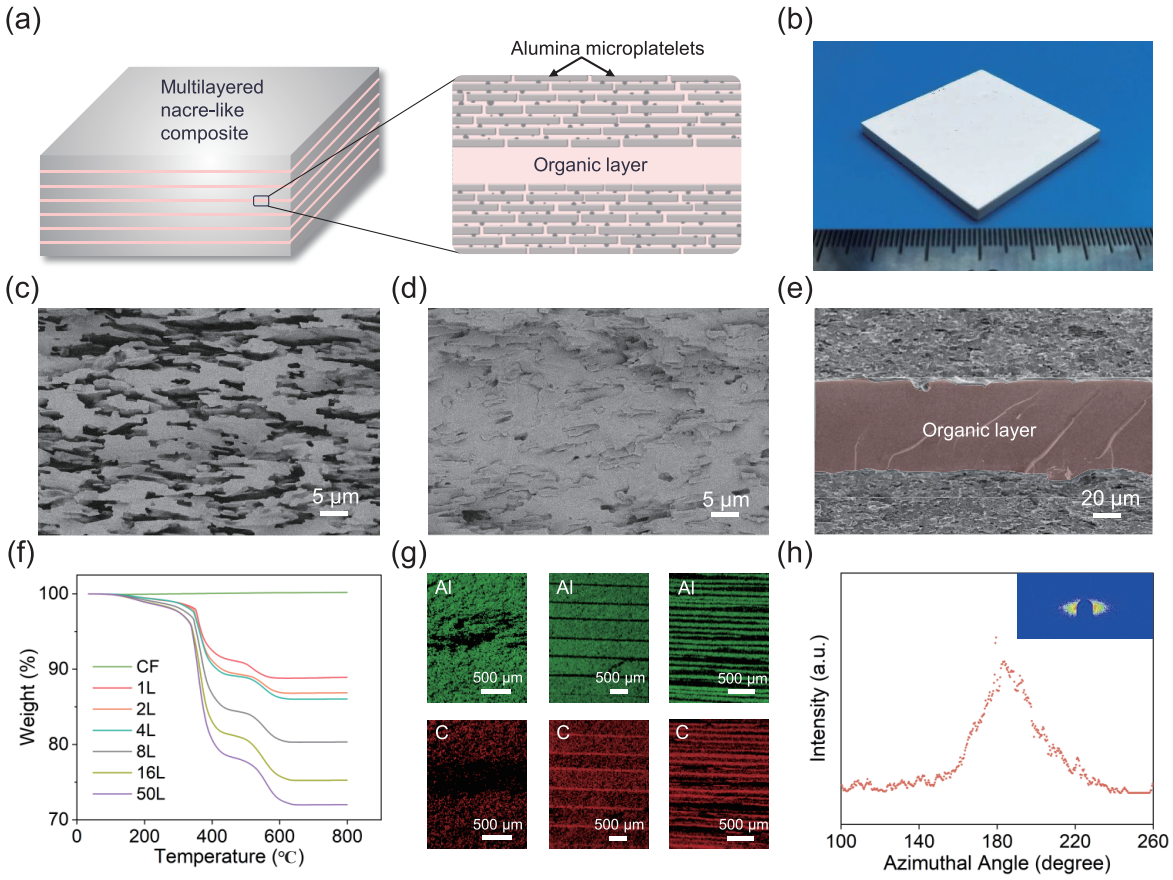

Fig. 1. Structural and mechanical characterization. (a) Schematic diagram of the hierarchically structured nacre-like composite. (b) Digital photos of a typical 50L composite. (c) Cross-sectional SEM image of a CF. (d) Cross-sectional SEM image of a CF after EP infiltration. (e) Cross-sectional SEM image showing the organic layer between adjacent brick-and-mortar lamellae. (f) TGA data of CF and multilayered composites. (g) EDS images showing cross-sections of the 1L, 8L and 50L composites. (h) 2D SAXS patterns of a 50L composite with an X-ray beam parallel to the layer direction.

organic content (Fig. 1f, Fig. S6). The energy dispersive X-ray spectroscopy (EDS) images illustrate the distribution of aluminum and carbon (Fig. 1g, Fig. S7), indicating the microscale multilayered laminate structure of the composites. The two-dimensional (2D) SAXS patterns (Fig. 1h, Fig. S8) validated the highly organized arrangement of alumina microplatelets within the multilayered composite.

3.2 Mechanical performance

3.2.1 Quasistatic mechanical performance of the multilayered nacre-like composites

Compression and bending tests were initially carried out to verify the efficacy of our hierarchical structural design for multilayered nacre-like composites under quasistatic loading conditions. Compared with those of pure CF, the results of compression tests indicated that the strengths and ductilities of the composites were greater (Fig. 2a, Fig. S9a). The composites exhibited different compressive mechanical properties along the two perpendicular loading directions (Fig. 2a, Fig. S9b), reflecting the anisotropy of the composites. We found that the compressive strength of the composites significantly decreased as the number of layers increased with loading direction perpendicular to the layers (Fig. 2b). This occurred because as the number of layers increased, the content of soft phase polymers in the composites increased (Fig. 1f). Three-point flexural tests demonstrated that both the flexural strength and flexural modulus of the composites were significantly greater than those of the pure organic phase and CF (Fig. 2c). After EP was penetrated, the flexural strength increased by approximately 3.66 times, and the flexural modulus improved by approximately 2.21 times. However, these two indicators declined simultaneously with increasing layer number (Fig. 2d).

By using a microscopic camera to observe the fracture processes of the CF, 1L composite and 50L composite samples during the SENB tests, we found that their fracture behaviors were quite different (Movies S1–S3 in Supporting information). At the microscale, long-range zig-zag crack deflection and the stretching of EP interlayers between adjacent brick-and-mortar lamellae in the 50L sample were clearly observed (Fig. 3a–d and Fig. S10). At the nanoscale, we also observed crack deflection at the crack tip (Fig. 3e), and the pull-out of microplatelets on the fracture surface was clearly observed (Fig. 3f). These fracture behaviors operate at different length scales and serve as potent extrinsic toughening mechanisms that relieve locally high stresses and increase crack resistance[26,29,32]. In contrast, the fracture surface of a pure CF displays a minor deflection (Fig. S11). Notably, an increase in the number of layers made it easier for the cracks to deflect

CSTR: 32290.14.JUSTC-2024-0163
DOI: 10.52396/JUSTC-2024-0163
JUSTC, **2025**, 55(6): 0604

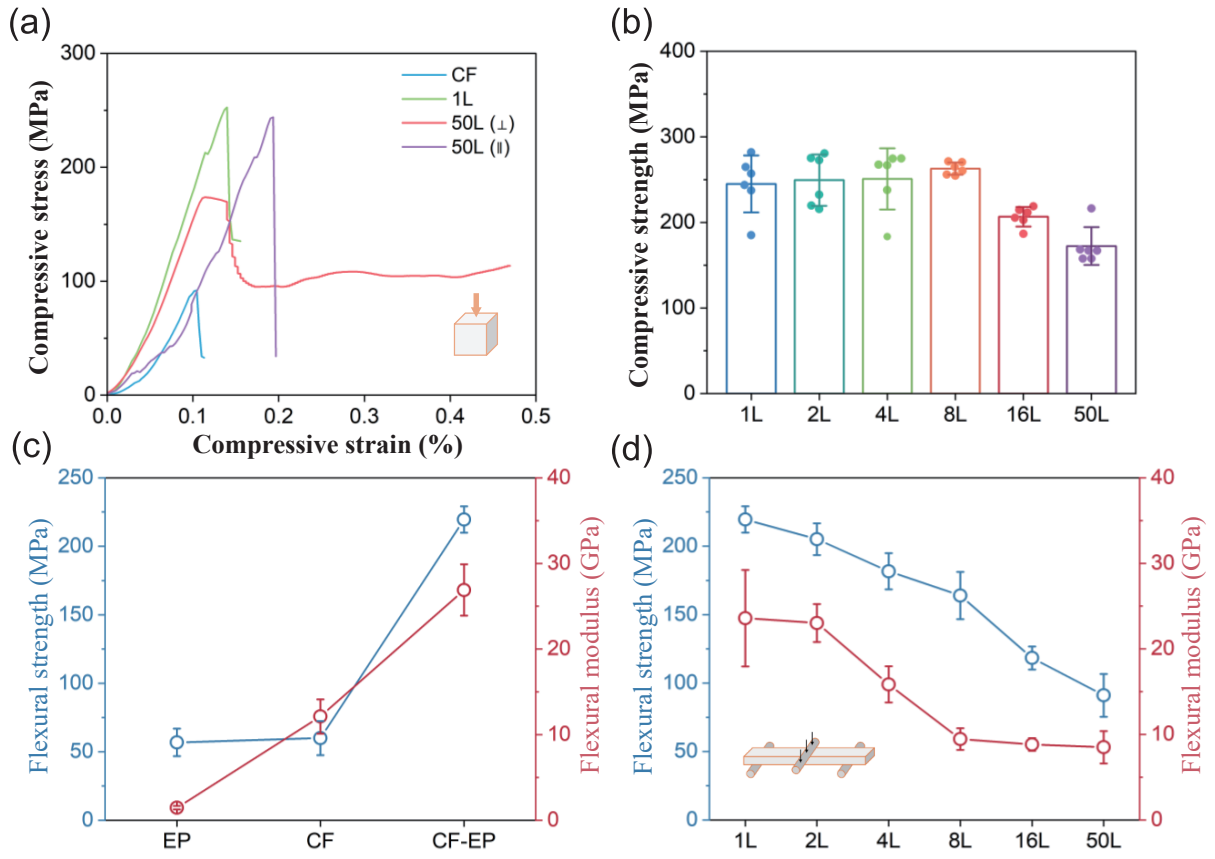

Fig. 2. Quasistatic mechanical performance. (a) Typical stress–strain curves for CF and 1L and 50L composites derived from compression tests. (⊥) indicates the loading direction perpendicular to the layers; (∥) indicates the loading direction parallel to the layers. (b) Comparison of the compressive strength of nacre-like composites with different numbers of layers. (c) Comparison of the flexural strength and modulus of EP, CF, and CF after EP infiltration (1L composite). (d) Comparison of the flexural strength and modulus of nacre-like composites with different numbers of layers.

along the rigid-soft interfaces during testing (Fig. S12). The mechanical responses and fracture characteristics of these samples suggest that the multilayered nacre-like composites are more advantageous for resisting crack initiation and propagation.

3.2.2 Dynamic mechanical performance of the multilayered nacre-like composites

Dynamic mechanical analysis was further performed to evaluate the impact-resistant and damping behavior of the multilayered nacre-like composites. The drop-ball rebound test revealed that the energy dissipation ratio of EP-CF (1L nacre-like composite) was significantly greater than that of pure EP and was equivalent to that of CF (Fig. 4a). This result indicated that the brick-and-mortar structure at the nanoscale effectively absorbed impact energy. The relatively high energy dissipation ratio of a CF may be due to damage to its internal porous microstructure. Moreover, we found that with increasing layer number, the energy dissipation ability of the composites became stronger (Fig. 4b and c). The energy dissipation ratio for the 50L composite reached approximately 85.63%. The drop-hammer impact test results displayed a pattern similar to that of the drop-ball rebound test results (Fig. 4d and e). Compared with the CF, the CF-EP (1L composite) provided more energy for breakthrough (Fig. 4d). Additionally, as the number of layers increased, their capacity to resist impact damage increased (Fig. 4e). The peak fracture energy of the 50L composites reached approximately 0.73 J. This result provided direct evidence for the effectiveness of the rigid–soft laminate structure at the microscale in enhancing the impact resistance of the multilayered nacre-like composite. Digital photographs and micro-CT images were further captured to display the damage to the nacre-like composites subsequent to the drop-hammer impact test (Fig. 4f and g). The micro-CT images of an impacted 50L composite revealed significant crack deflection inside it (Fig. 4g–k, Movie S4).

Furthermore, the damping characteristics of EP, CF and the nacre-like composites were examined by analyzing their storage modulus (E') and loss modulus (E'') within the frequency range of 20–80 Hz. Compared with those of pure EP and the CF, the storage modulus of the 1L composite was significantly greater (Fig. 5a), indicating that the infiltration of soft EP into the CF resulted in increased material stiffness. However, as the layer number increased, a decrease in the storage modulus of the composite was observed, suggesting a decrease in its stiffness (Fig. 5a). This finding is consistent with the changing trend of the composites under quasistatic bending loading (Fig. 2b). The stress–strain curves derived from the SHPB experiments indicate that the CF did not experience a postcompression disintegration process, whereas the 1L composites exhibited rapid disintegration (Fig. 5b). In

CSTR: 32290.14.JUSTC-2024-0163
DOI: 10.52396/JUSTC-2024-0163
JUSTC, **2025**, 55(6): 0604

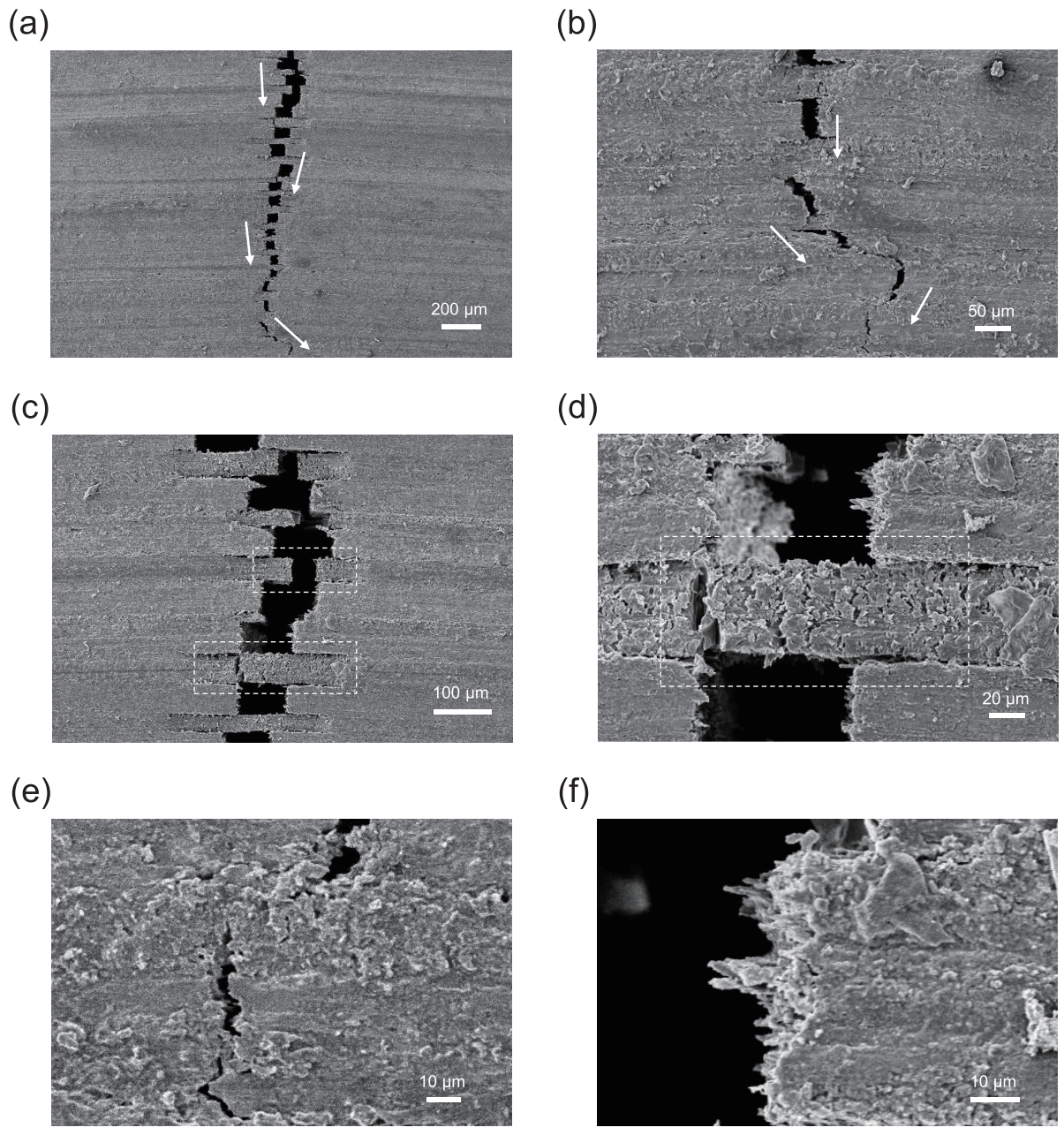

Fig. 3. Multiscale toughening mechanisms. (a, b) SEM images showing the long-range crack deflection morphology of a 50L composite after the SENB test. The white arrows indicate the extension direction of the crack. (c, d) SEM images showing the extensive plastic deformation of the polymer interlayers (typical polymer bridging) between adjacent brick-and-mortar lamellae, as depicted by the white dashed boxes. (e, f) SEM images showing nanoscale crack deflections at the crack tip and the pullout of alumina microplatelets on the fracture surface.

contrast, the 50L composite demonstrated an extended compression process. This result demonstrated that with increasing layer number, the composites displayed more pronounced plastic behavior rather than experiencing catastrophic failure. Therefore, we can infer that composites with hierarchically designed structures also have superior energy dissipation capabilities under high-speed impact load conditions.

4 Conclusions

In conclusion, we reported the manufacture of multilayered nacre-like composites via a scalable bottom-up assembly process and specifically evaluated their dynamic mechanical properties. By integrating the nanoscale nacreous brick-and-mortar structure with a microscale multilayered laminated structure, we produced hierarchically designed nacre-like composites. The hierarchically structured nacre-like composites incorporate toughening mechanisms at both the nanoscale and the microscale, thereby enhancing their macroscopic impact resistance. This work offers valuable insights for the upcoming development of impact-resistant composites and may yield more targeted design ideas for improving the dynamic impact resistance research of materials in the future.

CSTR: 32290.14.JUSTC-2024-0163
DOI: 10.52396/JUSTC-2024-0163
JUSTC, **2025**, 55(6): 0604

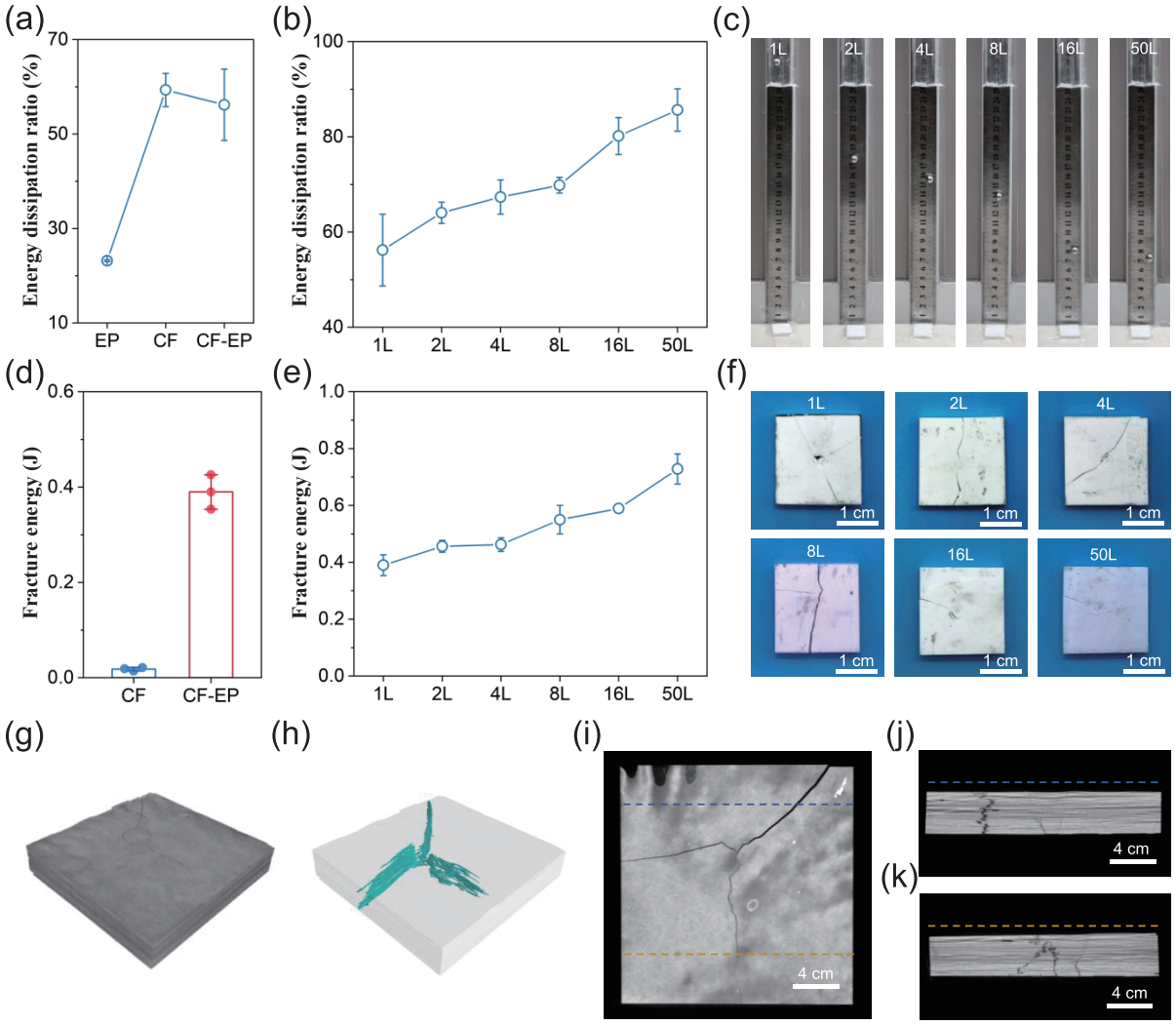

Fig. 4. Dynamic mechanical properties. (a, b) Comparison of the energy loss ratios of EP, CF and nacre-like composites with different numbers of layers from drop-ball rebound tests. (c) Digital photographs showing the final rebound heights of the balls falling through the nacre-like composites with different numbers of layers. (d, e) Comparison of the peak fracture energys of CF and nacre-like composites with different numbers of layers from drop-hammer impact tests. (f) Digital photographs showing the crack state of nacre-like composites with different numbers of layers when they are crushed by drop-hammer impact. (g–k) Micro-CT images showing the internal damage morphology of a typical 50L composite following the drop-hammer impact test (j and k show the cross-sectional damage morphologies of the sample marked with the blue dashed line and the yellow dashed line, respectively).

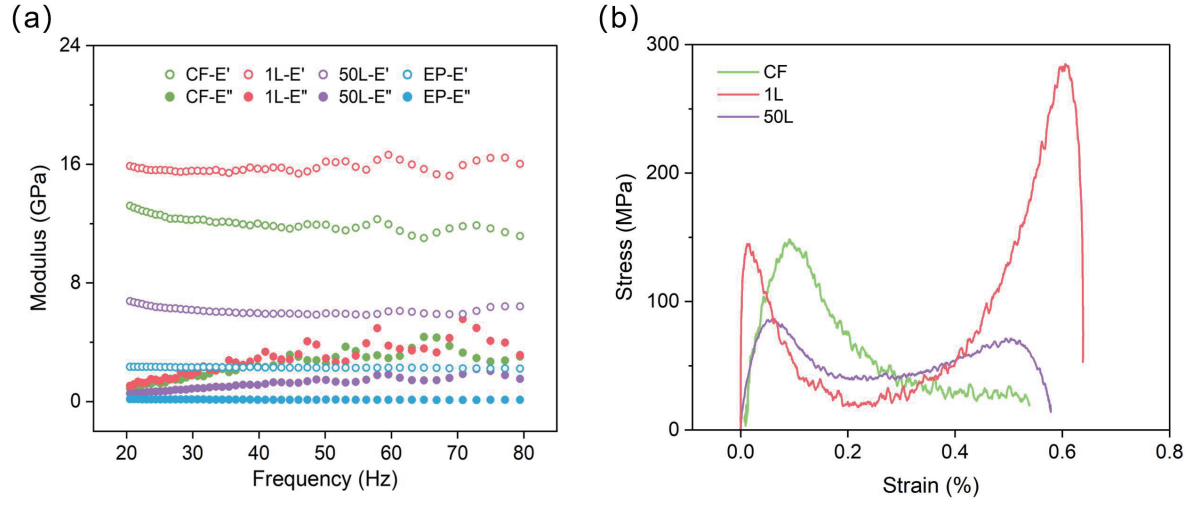

Fig. 5. Mechanical characterization. (a) Comparison of the storage modulus (E') and loss modulus (E'') of CF, EP, the 1L composite and the 50L composite. (b) Converted stress–strain diagrams of the CF, 1L, and 50L composites from the SHPB tests.

CSTR: 32290.14.JUSTC-2024-0163
DOI: 10.52396/JUSTC-2024-0163
JUSTC, **2025**, 55(6): 0604

Supporting information

The supporting information for this article can be found online at https://doi.org/10.52396/JUSTC-2024-0163. The supporting information includes twelve figures and four movies.

Acknowledgements

This work was supported by the Fundamental Research Funds for the Central Universities (WK2340000112), the National Key Research and Development Program of China (2021YFA0715700), and the National Natural Science Foundation of China (22222508, 22475205). The authors wish to acknowledge the Instruments Center for Physical Science of the University of Science and Technology of China. This work was partially carried out at the USTC Center for Micro- and Nanoscale Research and Fabrication.

Conflict of interest

The authors declare that they have no conflict of interest.

Biographies

Qingsheng Zeng is currently a graduate student at the School of Stomatology, Anhui Medical University. His research primarily focuses on the design, fabrication, and mechanical properties of biomimetic materials based on bioceramics.

Jiahao Su is currently a graduate student at the School of Stomatology, Anhui Medical University. His research primarily focuses on the design, fabrication, and mechanical properties of biomimetic materials based on bioceramics, and etiology of enamel related lesions.

Duohong Zou is currently an Associate Chief Physician, Professor, and Doctoral Supervisor in the Department of Oral Surgery at the Ninth People's Hospital affiliated with Shanghai Jiao Tong University School of Medicine. His research primarily focuses on the clinical and research work in dental implantology and maxillofacial reconstruction.

Huailing Gao is currently a Professor at the Department of Modern Mechanics, University of Science and Technology of China (USTC). He received his Ph.D. degree in Inorganic Chemistry from USTC in 2016. His research primarily focuses on the toughening and fatigue-resistant design, manufacturing, and mechanical properties research of biomimetic micro/nano-structured materials.

References

[1] Padture N P. Advanced structural ceramics in aerospace propulsion. *Nature Materials*, **2016**, *15*: 804–809.
[2] Kim J, Jia X. From space to battlefield: A new breed of multifunctional fiber sheets for extreme environments. *Matter*, **2020**, *3* (3): 602–604.
[3] Wen S M, Chen S M, Gao W, et al. Biomimetic gradient bouligand structure enhances impact resistance of ceramic-polymer composites. *Advanced Materials*, **2023**, *35* (21): 2211175.
[4] Gu G X, Takaffoli M, Buehler M J. Hierarchically enhanced impact resistance of bioinspired composites. *Advanced Materials*, **2017**, *29* (28): 1700060.
[5] Portela C M, Edwards B W, Veysset D, et al. Supersonic impact resilience of nanoarchitected carbon. *Nature Materials*, **2021**, *20*: 1491–1497.
[6] Zhao Q, Liang Y, Zhang Z, et al. Study on the impact resistance of bionic layered composite of TiC-TiB_2/Al from Al-Ti-B_4C system. *Materials*, **2016**, *9* (8): 708.
[7] Yin Z, Hannard F, Barthelat F. Impact-resistant nacre-like transparent materials. *Science*, **2019**, *364* (6447): 1260–1263.
[8] Ni J, Lin S, Qin Z, et al. Strong fatigue-resistant nanofibrous hydrogels inspired by lobster underbelly. *Matter*, **2021**, *4* (6): 1919–1934.
[9] Liang X, Chen G, Lei I M, et al. Impact-resistant hydrogels by harnessing 2D hierarchical structures. *Advanced Materials*, **2023**, *35* (1): 2207587.
[10] Gonzalez G M, Ward J, Song J, et al. *para*-Aramid fiber sheets for simultaneous mechanical and thermal protection in extreme environments. *Matter*, **2020**, *3* (3): 742–758.
[11] Ritchie R O. The conflicts between strength and toughness. *Nature Materials*, **2011**, *10*: 817–822.
[12] Wang X, Zhang Z, Liang Z, et al. Hybridizing shear-stiffening gel and chemically-strengthened ultrathin glass sheets for flexible impact-resistant armor. *Advanced Science*, **2024**, *11* (33): 2403379.
[13] Barthelat F, Yin Z, Buehler M J. Structure and mechanics of interfaces in biological materials. *Nature Reviews Materials*, **2016**, *1* (4): 16007.
[14] Ling S, Kaplan D L, Buehler M J. Nanofibrils in nature and materials engineering. *Nature Reviews Materials*, **2018**, *3*: 18016.
[15] Eder M, Amini S, Fratzl P. Biological composites —complex structures for functional diversity. *Science*, **2018**, *362* (6414): 543–547.
[16] Jia Z, Deng Z, Li L. Biomineralized materials as model systems for structural composites: 3D architecture. *Advanced Materials*, **2022**, *34* (20): 2106259.
[17] Wegst U G K, Bai H, Saiz E, et al. Bioinspired structural materials. *Nature Materials*, **2015**, *14*: 23–36.
[18] Nepal D, Kang S, Adstedt K M, et al. Hierarchically structured bioinspired nanocomposites. *Nature Materials*, **2023**, *22*: 18–35.
[19] Chen S M, Zhang Z B, Gao H L, et al. Bottom-up film-to-bulk assembly toward bioinspired bulk structural nanocomposites. *Advanced Materials*, **2024**, *36* (23): 2313443.
[20] Le Ferrand H, Bouville F, Niebel T P, et al. Magnetically assisted slip casting of bioinspired heterogeneous composites. *Nature Materials*, **2015**, *14*: 1172–1179.
[21] Gao H L, Chen S M, Mao L B, et al. Mass production of bulk artificial nacre with excellent mechanical properties. *Nature Communications*, **2017**, *8*: 287.
[22] Du G, Mao A, Yu J, et al. Nacre-mimetic composite with intrinsic self-healing and shape-programming capability. *Nature Communications*, **2019**, *10*: 800.
[23] Zhao C, Zhang P, Zhou J, et al. Layered nanocomposites by shear-flow-induced alignment of nanosheets. *Nature*, **2020**, *580*: 210–215.
[24] Wan S, Li X, Chen Y, et al. High-strength scalable MXene films through bridging-induced densification. *Science*, **2021**, *374* (6563): 96–99.
[25] Amini A, Khavari A, Barthelat F, et al. Centrifugation and index matching yield a strong and transparent bioinspired nacreous composite. *Science*, **2021**, *373* (6560): 1229–1234.
[26] Chen K, Tang X, Jia B, et al. Graphene oxide bulk material reinforced by heterophase platelets with multiscale interface crosslinking. *Nature Materials*, **2022**, *21*: 1121–1129.
[27] Meng Y F, Yu C X, Zhou L C, et al. Nanograded artificial nacre with efficient energy dissipation. *The Innovation*, **2023**, *4* (6): 100505.
[28] Wan S, Chen Y, Huang C, et al. Scalable ultrastrong MXene films with superior osteogenesis. *Nature*, **2024**, *634*: 1103–1110.
[29] Grossman M, Pivovarov D, Bouville F, et al. Hierarchical toughening of nacre-like composites. *Advanced Functional Materials*, **2019**, *29* (9): 1806800.
[30] Beese A M, An Z, Sarkar S, et al. Defect-tolerant nanocomposites through bio-inspired stiffness modulation. *Advanced Functional Materials*, **2014**, *24* (19): 2883–2891.
[31] Zhang Z B, Gao H L, Wen S M, et al. Scalable manufacturing of mechanical robust bioinspired ceramic–resin composites with locally tunable heterogeneous structures. *Advanced Materials*, **2023**, *35* (14): 2209510.
[32] Bouville F, Maire E, Meille S, et al. Strong, tough and stiff bioinspired ceramics from brittle constituents. *Nature Materials*, **2014**, *13*: 508–514.

CSTR: 32290.14.JUSTC-2024-0163
DOI: 10.52396/JUSTC-2024-0163
JUSTC, **2025**, 55(6): 0604